Noise Uncertainty in Cognitive Radio Sensing: Analytical Modeling and Detection Performance

Marwan A. Hammouda and Jon W. Wallace
Jacobs University Bremen
Campus Ring 1, 28759 Bremen, Germany
E-mail: m.hammouda@jacobs-university.de, wall@ieee.org

***Abstract*—Methods for primary user detection in cognitive radio may be severely impaired by noise uncertainty (NU) and the associated SNR wall phenomenon. The ability to avoid the SNR wall is proposed herein by detailed statistical modeling of the noise process when NU is present. A Gaussian model for the inverse noise standard deviation is proposed, and good agreement with the more common lognormal distribution is demonstrated for low to moderate noise uncertainty. Closed-form pdfs for a single noise sample and the energy of multiple noise samples are derived, allowing an optimal Neyman-Pearson detector to be employed when NU is present, thus avoiding the SNR wall effect. Initial measurements are presented that explore energy detection at low SNR in a practical system, showing that the noise distribution can be easily calibrated (learned) using a switch and matched load in the receiver. Useful detection performance down to -16 dB with energy detection is demonstrated, and it is found that noise uncertainty is not significant for an instrument-grade low-noise amplifier (LNA) for sub-minute acquisition times.**

I. Introduction

Cognitive radio [1] is an interesting emerging paradigm for radio networks, where radios are able to sense and exploit unused spectral resources, ideally improving spectrum utilization and allowing networks to operate in a more decentralized fashion. In the absence of cooperating primary users or beacons that indicate local spectrum usage, overlay-based cognitive radios must have sensing hardware and algorithms that are robust in the sense of providing very low missed detection rates at low SNR, thus impacting existing licensed users negligibly.

Assuming an ideal noise model and given enough sensing time, simple methods like energy detection can theoretically discriminate the presence of a primary transmitter, even at very low SNR. In [2] the important effect of uncertainty in the noise distribution was identified and studied in detail, proving that when noise variance is confined to an interval but otherwise unknown, an *SNR wall* exists, below which useful detection performance cannot be guaranteed regardless of the observation time.

The purpose of this paper is to study whether the SNR wall phenomenon can be eased by more detailed modeling of the noise uncertainty (NU) and to explore the impact of NU through direct measurement. It is argued in [2] that noise calibration to learn the noise model is not possible in cognitive radio since a primary may be present that corrupts any noise measurements. However, the dominant noise in RF systems is typically generated in the front-end amplifier and not the antenna. Thus, the noise level can be periodically measured by switching the receiver input to a matched load where primary signal is not present. Even then, the noise measurement may have error, but it is shown herein that with proper modeling of that error, the SNR wall can be reduced dramatically.

The remainder of the paper is organized as follows. Section II provides some background on energy detection and reviews the SNR wall phenomenon. Section III defines the noise uncertainty model and derives closed-form noise pdfs in the presence of NU. Section IV provides numerical examples that illustrate how noise calibration can provide useful detection performance, whereas ignoring detection performance leads to an SNR wall. Section V presents initial measurements showing that energy detection at very low SNR is practically possible with the noise calibration technique. Finally, Section VI provides some concluding remarks.

II. Background

This section briefly reviews concepts on optimal detection, energy detection, and noise uncertainty that are required for the remainder of the paper.

The problem of primary detection in cognitive radio is usually treated using classical detection theory [3], where a decision must be made among two hypotheses: (H_0) only noise is present, or (H_1) signal plus noise is present. The received waveform x_n under these two hypotheses is

$$\begin{aligned} \mathrm{H}_0 &: x_n = w_n, \qquad n = 1, 2, \ldots, N \\ \mathrm{H}_1 &: x_n = w_n + s_n, \quad n = 1, 2, \ldots, N \end{aligned} \tag{1}$$

where w_n and s_n are the nth real noise and signal samples, respectively, and the detector must select H_0 or H_1 based only on observation of x_n for $n = 1, \ldots, N$. Given a decision rule, P_d is the probability of detection, or the probability that the detector correctly declares H_1, whereas P_fa is the the probability of false alarm, or the probability that the detector declares H_1 when the true hypothesis is H_0.

When the pdfs of the received waveform x_n under hypotheses H_0 and H_1 are known, the Neyman-Pearson (N-P) detector provides optimal detection performance in the sense of providing maximum P_d for fixed P_fa. The N-P detector employs a likelihood ratio test (LRT), given by

$$\mathcal{L}(\mathbf{x}) = \frac{f_{H_1}(\mathbf{x})}{f_{H_0}(\mathbf{x})}, \tag{2}$$

978-1-4577-1924-0/12/$26.00 ©2012 IEEE

where $f_H(\mathbf{x})$ is the joint pdf of the observed samples for hypothesis H. For a selected threshold λ, the detector declares H_1 when $\mathcal{L}(\mathbf{x}) \geq \lambda$, otherwise it declares H_0. The threshold can be computed by fixing P_{fa} and inverting the cdf for the H_0 (noise only) hypothesis.

When noise and signal are both i.i.d. Gaussian, the energy of the signal, given by

$$p = \sum_{n=1}^{N} x_n^2, \tag{3}$$

is a sufficient statistic. Detection based on p is known as energy detection, and the distribution of p is given by the Chi-Squared distribution, allowing the required LRT threshold and resulting detection performance to be computed in closed form. Given that the variance $\sigma_0^2 = \mathrm{Var}(w_n)$ is known, the energy detector can eventually provide near-perfect detection if N is made large enough, even at very low SNR.

Unfortunately, a practical system will only have an estimate of σ_0^2, and this imperfect knowledge is referred to as noise uncertainty (NU). The NU concept was identified and studied in detail in [2], where noise variance is assumed to be confined to the interval $[\sigma_{\mathrm{lo}}^2, \sigma_{\mathrm{hi}}^2]$ but otherwise unknown. In this case, worst-case detection performance for the N-P detector can be computed by assuming

$$\sigma_0^2 = \begin{cases} \sigma_{\mathrm{hi}}^2, & \text{under } \mathrm{H}_0, \\ \sigma_{\mathrm{lo}}^2, & \text{under } \mathrm{H}_1, \end{cases} \tag{4}$$

thus providing the minimum separation of the H_0 and H_1 pdfs. For a given noise interval, as the SNR is lowered a threshold is reached below which the worst-case energy detector exhibits $P_{\mathrm{d}} < P_{\mathrm{fa}}$ regardless of the number of samples. This complete detection failure is referred to as the SNR wall.

III. Noise Uncertainty Modeling

The main idea of this paper is to overcome the SNR wall phenomenon by more detailed modeling of the noise uncertainty. In this work, noise and signal are modeled as conditional Gaussian processes where a single real sample x_n has the conditional distribution

$$f(x_n|\alpha) = \frac{\alpha}{\sqrt{2\pi}} \exp\{-\alpha^2 x_n^2/2\}, \tag{5}$$

$\alpha = 1/\sigma$, and σ^2 is the variance. Note that the choice of using α rather than σ as the modeled noise parameter in this work avoids having integration variables in the denominator, thus simplifying closed-form analysis. Given an i.i.d. process where α is fixed for a short time consisting of N samples, the marginal pdf of the vector $\mathbf{x}$ is

$$f(\mathbf{x}) = \frac{1}{(2\pi)^{N/2}} \int_0^\infty f(\alpha)\alpha^N \exp\left\{-\frac{\alpha^2}{2}\sum_{n=1}^{N} x_n^2\right\} d\alpha, \tag{6}$$

where $f(\alpha)$ is the pdf of the unknown noise parameter α. Since the energy $p = \sum_{n=1}^{N} x_n^2$ is a sufficient decision statistic here, we concentrate on this parameter.

The distribution of p conditioned on α is given by the Chi-Squared distribution, or

$$f(p|\alpha) = \frac{\alpha^2}{2^{N/2}\Gamma(N/2)}(\alpha^2 p)^{N/2-1} \exp\{-\alpha^2 p/2\}, \tag{7}$$

and the marginal distribution $f(p)$ therefore becomes

$$f(p) = \frac{1}{2^{N/2}\Gamma(N/2)} \int_0^\infty f(\alpha)\alpha^2(\alpha^2 p)^{N/2-1} \exp\{-\alpha^2 p/2\}\, d\alpha. \tag{8}$$

The idea of this paper is to choose a distribution for the inverse noise level $f(\alpha)$ that not only can be used to calibrate a practical system, but also has a simple form allowing (8) to be derived in closed form.

The lognormal distribution is often proposed for modeling the variance of fading and noise processes, in which case $f(\sigma)$ is expressed as

$$f_{\mathrm{LN}}(\sigma) = \frac{1}{\sigma\sqrt{2\pi}\sigma_{\mathrm{LN}}} \exp\left\{-\frac{1}{2}(\log\sigma - \mu_{\mathrm{LN}})^2/\sigma_{\mathrm{LN}}^2\right\}. \tag{9}$$

where μ_{LN} and σ_{LN} are the mean and standard deviation of $\log\sigma$. Expressed in dB units $\mu_{\mathrm{LN}} = \delta\mu_{\mathrm{dB}}$ and $\sigma_{\mathrm{LN}} = \delta\sigma_{\mathrm{dB}}$, where $\delta = \log(10)/20$. Letting $\alpha = 1/\sigma$, (9) can be transformed to

$$f_{\mathrm{LN}}(\alpha) = \frac{1}{\alpha\sigma_{\mathrm{LN}}\sqrt{2\pi}} \exp\left\{-\frac{1}{2}(\log\alpha + \mu_{\mathrm{LN}})^2/\sigma_{\mathrm{LN}}^2\right\}, \tag{10}$$

which differs from (9) only in the sign of μ_{LN}. A major drawback of the lognormal distribution, however, is that closed-form analysis is often difficult.

For small levels of noise uncertainty, we consider a much simpler model, where $f(\alpha)$ is assumed to be Gaussian which is fit to (10) using closed-form expressions for the mean and variance of (10) given by

$$\mu_\alpha = \mathrm{E}\{\alpha\} = \exp\{-\mu_{\mathrm{LN}} + \sigma_{\mathrm{LN}}^2/2\}, \tag{11}$$

$$\sigma_\alpha = \mathrm{Std}\{\alpha\} = [\exp(\sigma_{\mathrm{LN}}^2) - 1]\exp(-2\mu_{\mathrm{LN}} + \sigma_{\mathrm{LN}}^2), \tag{12}$$

where $\mathrm{Std}(\cdot)$ denotes standard deviation. The pdf $f(\alpha)$ is then given by

$$f(\alpha) = \begin{cases} \dfrac{1}{C_\alpha\sqrt{2\pi}\sigma_\alpha} \exp\left\{-\dfrac{1}{2}\dfrac{(\alpha-\mu_\alpha)^2}{\sigma_\alpha^2}\right\}, & \alpha > 0, \\ 0, & \text{otherwise}, \end{cases} \tag{13}$$

where the rescaling constant $C_\alpha = \mathrm{erfc}[-\mu_\alpha/(\sqrt{2\sigma_\alpha^2})]/2$ results from the truncation of the left tail of the Gaussian at $\alpha = 0$ and $\mathrm{erfc}(\cdot)$ is the complementary error function. Note $C_\alpha \approx 1$ is omitted from later derivations, but it should be included if exact expressions are required.

A. Single Sample: Marginal Distribution

Assuming the Gaussian model for $f(\alpha)$, the marginal distribution of a single real sample is $f(x) = \int_0^\infty f(\alpha)f(x|\alpha)d\alpha$, or

$$f(x) = \frac{1}{2\pi\sigma_\alpha} \int_0^\infty \alpha e^{-\alpha^2 x^2/2} e^{-(\alpha-\mu_\alpha)^2/(2\sigma_\alpha^2)}\, d\alpha, \tag{14}$$

$$= \frac{1}{2\pi\sigma_\alpha} \int_0^\infty \alpha e^{-[a\alpha^2 - b\alpha + c]}\, d\alpha, \tag{15}$$

where

$$a = \frac{x^2}{2} + \frac{1}{2\sigma_\alpha^2}, \tag{16}$$

$$b = \mu_\alpha/\sigma_\alpha^2, \tag{17}$$

$$c = \mu_\alpha^2/(2\sigma_\alpha^2). \tag{18}$$

The integral is of the form of the error function, which can be obtained by completing the square, resulting in

$$f(x) = \frac{e^{-c_3}}{4\pi\sigma_\alpha}\left[\frac{e^{-c_1c_2^2}}{c_1} + \sqrt{\frac{\pi}{c_1}}\text{erfc}(-\sqrt{c_1}c_2)c_2\right], \tag{19}$$

where

$$c_1 = a, \tag{20}$$

$$c_2 = \mu_\alpha/(\sigma_\alpha^2x^2 + 1), \tag{21}$$

$$c_3 = \frac{1}{2}\frac{\mu_\alpha^2}{\sigma_\alpha^2}\left[1 - \frac{1}{\sigma_\alpha^2x^2 + 1}\right]. \tag{22}$$

B. Multiple Samples: Energy Distribution

For multiple independent samples, we will consider only the distribution of the energy p, which is a sufficient statistic whose distribution (8) becomes

$$f(p) = \frac{1}{2^{N/2}\Gamma(N/2)} \tag{23}$$

$$\times \int_0^\infty \frac{1}{\sqrt{2\pi}\sigma_\alpha} e^{-(\alpha-\mu_\alpha)^2/(2\sigma_\alpha^2)}\alpha^2(\alpha^2p)^{N/2-1}e^{-\alpha^2p/2}\ d\alpha, \tag{24}$$

$$= c_0\int_0^\infty \alpha^N e^{-(a\alpha^2-b\alpha+c)}\ d\alpha, \tag{25}$$

$$= c_0\int_0^\infty \alpha^N e^{-c_1(\alpha-c_2)^2-c_3}\ d\alpha, \tag{26}$$

$$= c_0e^{-c_3}\int_{-c_2}^\infty (\alpha+c_2)^N e^{-c_1\alpha^2}\ d\alpha, \tag{27}$$

$$= c_0e^{-c_3}\sum_{k=0}^N \binom{N}{k} c_2^k \underbrace{\int_{-c_2}^\infty \alpha^{N-k}e^{-c_1\alpha^2}\ d\alpha}_{I}, \tag{28}$$

where

$$a = c_1 = \frac{p}{2} + \frac{1}{2\sigma_\alpha^2}, \tag{29}$$

$$b = \mu_\alpha/\sigma_\alpha^2, \tag{30}$$

$$c = \mu_\alpha^2/(2\sigma_\alpha^2), \tag{31}$$

$$c_0 = \frac{p^{N/2-1}}{2^{N/2}\Gamma(N/2)\sqrt{2\pi}\sigma_\alpha} \tag{32}$$

$$c_2 = \mu_\alpha/(\sigma_\alpha^2p + 1) \tag{33}$$

$$c_3 = \frac{1}{2}\frac{\mu_\alpha^2}{\sigma_\alpha^2}\left[1 - \frac{1}{\sigma_\alpha^2p + 1}\right]. \tag{34}$$

The integral $I = I_1 + I_2$ can be evaluated by letting I_1 and I_2 be the contribution from α on the negative and positive axes, respectively, followed by the substitution $u = c_1\alpha^2$:

$$I_1 = (-1)^{N-k}\int_0^{c_2} \alpha^{N-k}e^{-c_1\alpha^2}\ d\alpha, \tag{35}$$

$$= \frac{(-1)^{N-k}}{2c_1^{L_k}}\underbrace{\int_0^{c_1c_2^2} u^{(N-k-1)/2}e^{-u}\ du}_{\Gamma(L_k, c_1c_2^2)\Gamma(L_k)}, \tag{36}$$

where $L_k = (N + 1 - k)/2$, and

$$\Gamma(a, x) = \frac{1}{\Gamma(a)}\int_0^x e^{-t}t^{a-1}\ dt \tag{37}$$

is the incomplete Gamma function. Similarly,

$$I_2 = \int_0^\infty \alpha^{N-k}e^{-c_1\alpha^2}\ d\alpha = \frac{1}{2c_1^{L_k}}\Gamma(L_k). \tag{38}$$

Combining results in

$$f(p) = \frac{c_0e^{-c_3}}{2}\sum_{k=0}^N \binom{N}{k}\frac{c_2^k}{c_1^{L_k}}\Gamma(L_k)\left[1 + (-1)^{N-k}\Gamma\left(L_k, c_1c_2^2\right)\right]. \tag{39}$$

C. Comparison of Gaussian and Lognormal

It is instructive to consider in what situations the Gaussian assumption for $f(\alpha)$ provides a reasonable model. Figure 1 plots $f(\alpha)$ side-by-side with $f(x)$ (single sample) for $\mu_{\text{dB}} = 0$ dB and different values of $\sigma_{\text{dB}} \in \{0.5$ dB, 1.0 dB, 2.0 dB$\}$. A log scale is used for $f(x)$ to highlight the small differences in the distribution tails. For small and moderate levels of noise uncertainty, the Gaussian approximation for $f(\alpha)$ is very close to the lognormal model. Also, for low noise uncertainty, the small mismatch in $f(\alpha)$ results in negligible error in the marginal density $f(x)$. For larger noise uncertainty, significant differences in the two models can be seen.

IV. Detection With NU

In this section we demonstrate with a simple example how having a model of the noise uncertainty can increase detection performance and remove the SNR wall. In this example, α is considered to be an unknown parameter following a lognormal distribution with μ_{dB} =0 dB and σ_{dB}=1 dB, which is subsequently fit using a Gaussian distribution. Signal and noise variance are assumed to be equal (SNR=0 dB) and $N = 20$ samples are used for detection.

First, a worst-case analysis like that presented in [2] is considered. Here, only bounds are set on the noise level, and the structure of the noise variation is ignored. It is assumed that the worst-case values for α are $\mu_\alpha \pm 1.5\sigma_\alpha$, which is conservative since the α will sometimes fall outside of these bounds. Figure 2 shows the Chi-Squared pdfs for the worst case assumption (4), indicating that detection is not possible since the H_0 curve is actually to the right of the H_1 curve.

Next, the structure of the noise error in (39) is taken into account, producing the pdfs in Figure 3 and indicating sufficient separation for useful detection. Figure 4 shows the detection performance from the worst case analysis and the case that

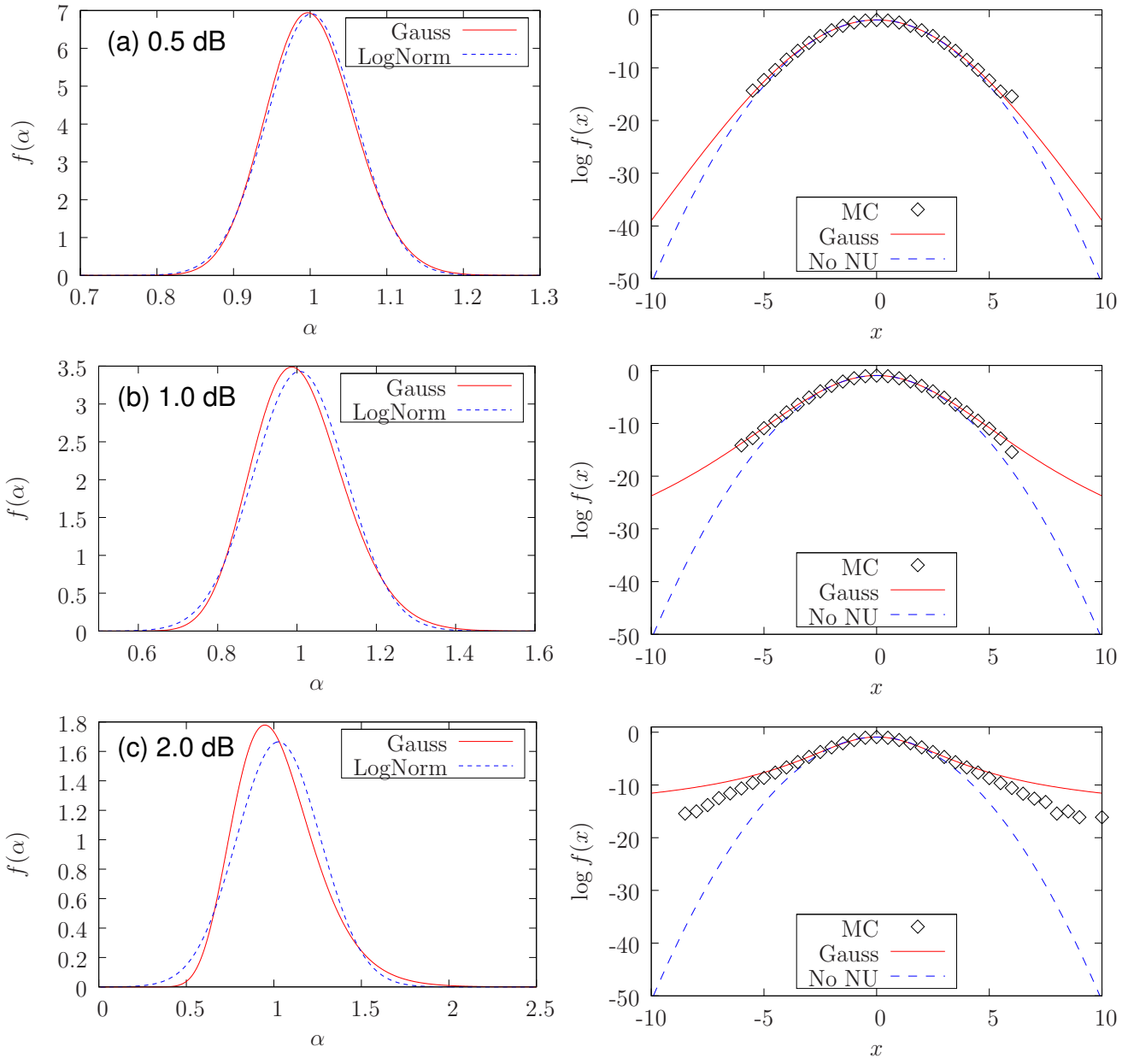

Fig. 1. A comparison of the lognormal distribution on α and a Gaussian approximation of the same distribution for different levels of noise uncertainty: $\sigma_{dB} \in \{0.5 \text{ dB}, 1.0 \text{ dB}, 2.0 \text{ dB}\}$. The noise uncertainty pdf $f(\alpha)$ is plotted on the left, and the corresponding marginal single sample pdf $f(x)$ is plotted on the right for each level of noise uncertainty. MC gives the results of Monte-Carlo simulations of the exact distribution with lognormal NU, compared with the Gaussian NU approximation (Gauss), and no noise uncertainty (No NU).

exploits the noise error pdf. In the worst-case analysis, the SNR wall has clearly been crossed, since $P_{\text{d}} < P_{\text{fa}}$. On the other hand, exploiting the known statistics of the noise error allows useful detection even when the exact noise level is uncertain.

V. Noise Calibration Measurement

In this section we present the results of an experiment that tests the possibility of energy detection at low SNR using practical hardware. As indicated in [2], noise calibration can be difficult in traditional wireless receivers where it is unknown if the primary is present or not. However, since most of the noise in a true receiver comes from the front-end low-noise-amplifier (LNA), the simple architecture depicted in Figure 5(a) can be used for noise calibration. To learn the noise distribution, the cognitive radio node periodically switches the receive channel away from the antenna to the matched termination to sample and learn the noise distribution.

This idea was tested using the experimental setup shown schematically in Figure 5(b). The setup employs a custom multiple-input multiple-output (MIMO) channel sounder that is basically equivalent to that presented in [4], with the

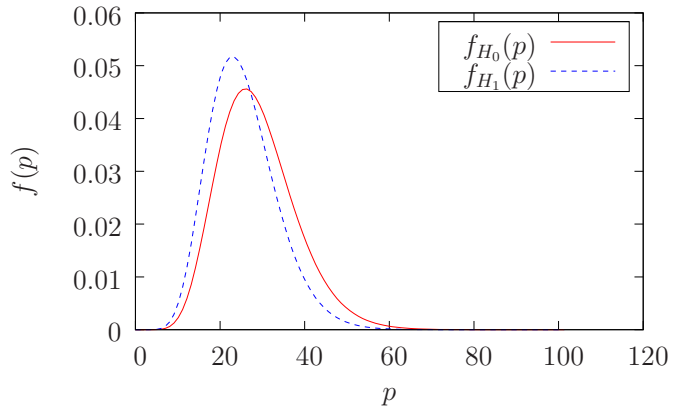

Fig. 2. Distribution of $f(p)$ for noise (H_0) and signal plus noise (H_1) assuming a worst-case model on the noise variation

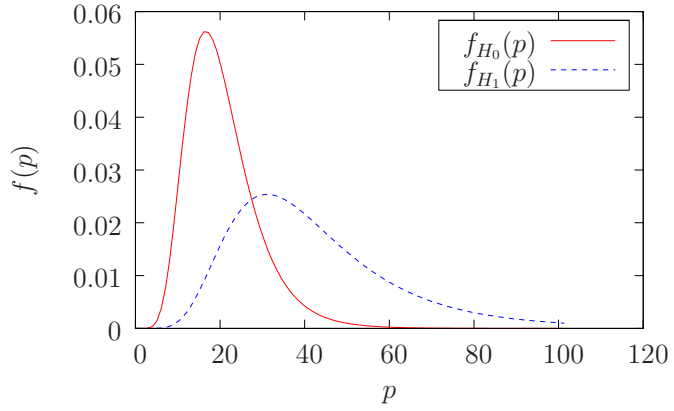

Fig. 3. Distribution of $f(p)$ for noise (H_0) and signal plus noise (H_1) using the proposed Gaussian NU model

exception that custom FPGA-based data acquisition is used in the present system.

The transmit (TX) node simulates the primary user, where a baseband Gaussian signal with a flat $W = 20$ MHz bandwidth is generated in 100 μs frames with the arbitrary waveform generator (AWG), up-converted to 2.55 GHz, power amplified to 23 dBm, and fed to either the active transmit channel (TX1) or a matched load (TX0). The channel is a simple direct cable connection from the transmitter to receiver, where different fixed attenuators are inserted giving loss L and producing different SNR levels at the receiver.

The receive (RX) node simulates the cognitive radio that employs a switch to feed its single receive chain either from the channel (RX1) or from a matched load (RX0). The receive chain consists of a 40 dB wideband LNA, down-conversion to a 50 MHz IF, followed by FPGA-based $f_s = 200$ MS/s data-acquisition. For this experiment, the raw IF samples are stored, passed to a PC, down-converted to complex baseband, and filtered (20 MHz bandwidth) using MATLAB before performing energy detection.

A total of M data records are acquired during each measurement, where the mth record is depicted in Figure 5(c).

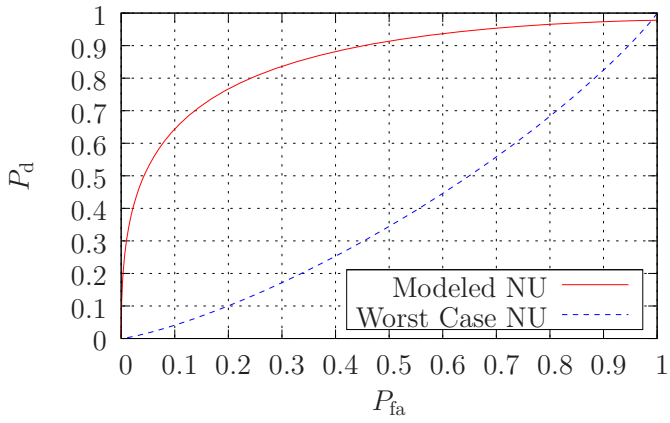

Fig. 4. Probability of detection P_d versus probability of false alarm P_{fa} for the worst-case assumption and the proposed NU model

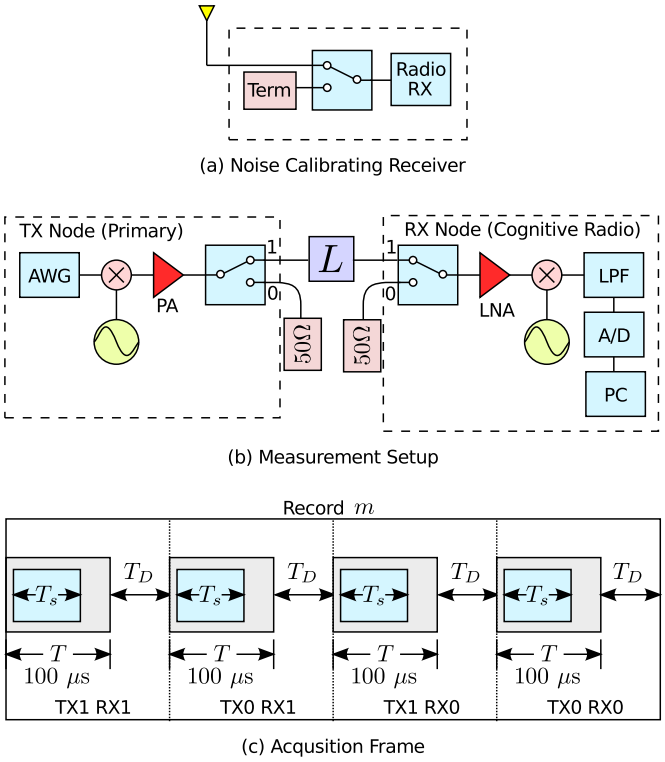

Fig. 5. Measurement setup for experimental study: (a) envisioned cognitive radio employing noise calibration, (b) channel sounder based acquisition system for experiment, (c) acquisition frame structure

Four phases are used in each record to probe all four switch combinations. Within a single phase, the channel is acquired for $T = 100$ μs followed by a delay of T_D, where $T_D = 0$ can be used for back-to-back acquisition. During post-processing, only N_s samples within each acquisition window are used, thus spanning time $T_s = N_s/f_s$ in order to simulate different integration windows in a cognitive radio energy detector. We will denote the nth filtered complex-baseband sample, of the kth phase, in the mth record as $x_{m,k,n}$. The four phases are denoted symbolically as $k \in$ {TX1 RX1, TX0 RX1, TX1 RX0,

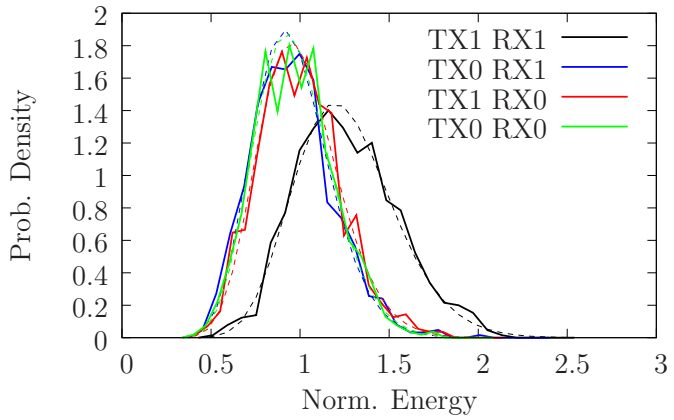

Fig. 6. Empirical pdfs (solid lines) for the four measurement phases with parameters: T_D=0, L=110 dB ($\rho = -6$ dB), $N_s = 100$, and $M = 800$ realizations. Fitted stationary Chi-Squared distributions are also shown (dashed lines).

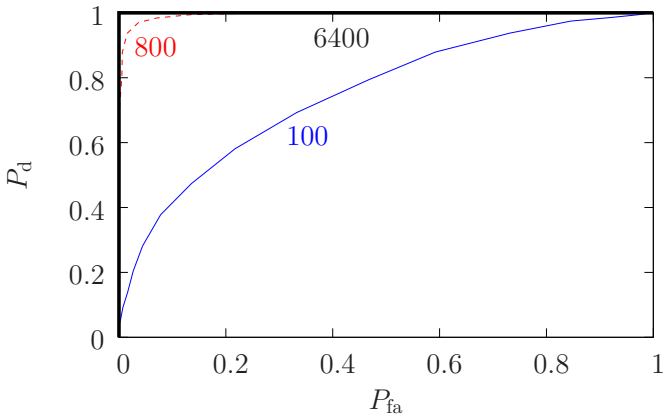

Fig. 7. Probability of detection (P_d) versus probability of false alarm (P_{fa}) for $T_D = 0$, $L = 110$ dB ($\rho = -6$ dB), and $N_s \in \{100,800,6400\}$.

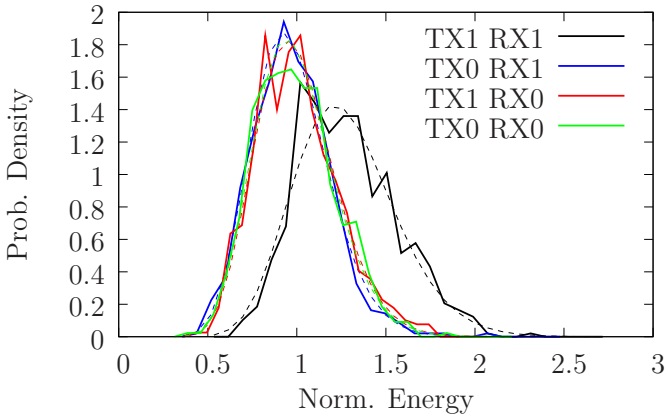

Fig. 8. Empirical pdfs (solid lines) for the four measurement phases with parameters: T_D=24 ms, L=110 dB ($\rho = -6$ dB), $N_s = 100$, and $M = 600$ realizations. Fitted stationary Chi-Squared distributions are also shown (dashed lines).

TX0 RX0}.

The energy in each record is computed using a variable window size N_s according to simple integration, or

$$p_{m,k} = \sum_{n=N_1+1}^{N_1+N_s} |x_{m,k,n}|^2, \tag{40}$$

where $N_1 = 50$ samples are always skipped at the beginning of each frame to avoid artifacts from the switching operations. Empirical distributions of the noise and signal plus noise energy are finally computed with a histogram using the M energy snapshots in (40).

Empirical signal and noise pdfs are also compared with ideal Chi-Squared pdfs with $N = 2WN_s/f_s$ degrees of freedom with sample variance estimated according to

$$\sigma_k^2 = \frac{1}{N_s M} \sum_{m=1}^{M} p_{m,k}. \tag{41}$$

The SNR (ρ) in dB is estimated at an attenuation level of L =80 dB (high SNR) using

$$\rho(L = 80 \text{ dB}) = 10 \log_{10} \left(\frac{\sigma^2_{\text{TX1RX1}}}{\sigma^2_{\text{TX1RX0}}} \right), \tag{42}$$

and SNR at lower attenuation levels is computed using $\rho(L) = \rho(L = 80 \text{ dB}) + 80 - L$. Note that for convenience, pdfs are normalized with respect to the expected noise energy $\sigma^2_{\text{TX1RX0}} N_s$.

Figure 6 plots empirical noise/signal pdfs for the four phases compared with Chi-Squared pdfs for $T_D = 0$ (back-to-back acquisition), $L = 110$ dB ($\rho = -6$ dB), and $N_s = 100$ samples ($N = 40$). First, the simple Chi-Squared distribution (no noise uncertainty) provides a good fit to the empirical pdfs for all cases, suggesting that the noise parameter α is fairly constant over the total acquisition time of $4TM = 320$ ms. Also, there is no apparent difference in the energy pdfs for the three noise-only (H_0) phases, indicating that having the RX connected to a matched load (TX1 RX0 and TX0 RX0) is equivalent to measuring the channel with the transmitter not present (TX0 RX1). Finally, good separation of the pdfs for the H_0 phase and H_1 phase (TX1 RX1) is demonstrated, indicating that useful detection with the direct noise measurement is possible.

Figure 7 plots probability of detection P_d versus probability of false alarm P_{fa} for the same case, computed directly from the empirical pdfs, where phase TX1 RX0 is used to estimate hypothesis H_0. The result shows that when the noise distribution is measured, near perfect detection is possible if the sample size is made large enough.

Figure 8 plots the empirical pdfs of the four phases for the same case, but with a longer delay between acquisitions $T_D = 24$ ms. Although we expected that increased noise uncertainty would result and spread the pdfs for the longer acquisition time of $4(T_D + T)M = 58$ s, they still exhibit an excellent fit to the simple Chi-Squared distribution with no noise uncertainty. Possible reasons that the noise process is so stable is that an instrument-grade LNA is used and the temperature in the channel sounder was likely very constant. In the future, we intend to study inexpensive consumer-grade

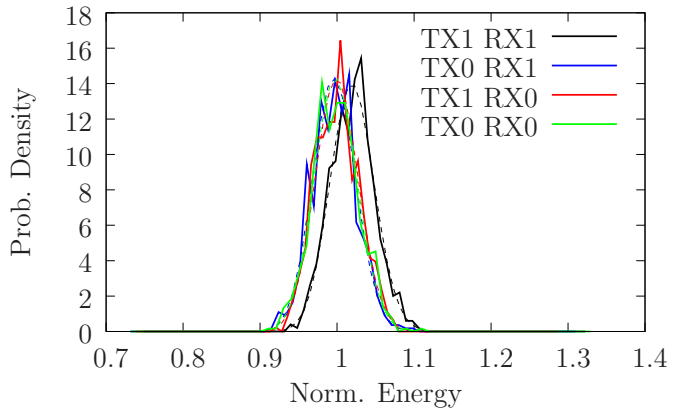

Fig. 9. Empirical pdfs (solid lines) for the four measurement phases with parameters: T_D=24 ms, $L = 120$ dB ($\rho = -16$ dB), $N_s = 6400$, and $M = 600$ realizations. Fitted stationary Chi-Squared distributions are also shown (dashed lines).

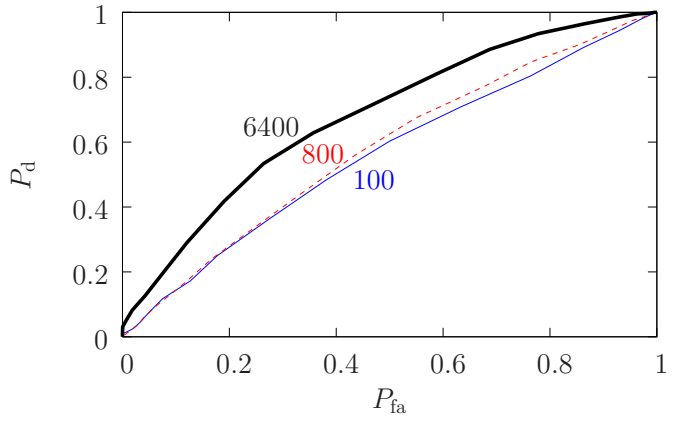

Fig. 10. Probability of detection (P_d) versus probability of false alarm (P_{fa}) for $T_D = 0$, $L = 120$ dB ($\rho = -16$ dB), and $N_s \in \{100,800,6400\}$ samples

LNAs under varying environmental conditions, where noise uncertainty is more likely to occur and noise calibration is more challenging.

Figure 9 shows pdfs for the case of lower SNR $L = 120$ dB ($\rho = -16$ dB), $T_D = 24$ ms, and $N_s = 6400$ samples. Even though the separation of the pdfs is poorer in this case, the detection performance plotted in Figure 10 indicates that the SNR wall effect is avoided, and useful detection is still possible with a long enough integration time.

In the future, the system will be modified to allow longer integration times where the effects of noise uncertainty are more likely to be observed. However, these results suggest that detection at SNRs of -16 dB or lower should be possible using simple noise calibration.

VI. Conclusion

Although noise uncertainty can be a severe impairment to robust detection in cognitive radio at low SNR, this paper has shown that the SNR wall effect can be overcome by proper specification of the noise variation. A closed-form pdf that assumes a Gaussian distribution for the inverse noise standard deviation was derived and it was shown that the model provides a good fit to the more commonly assumed lognormal pdf for low to moderate noise uncertainty. A simulation example was presented, confirming that by properly modeling the noise uncertainty, the SNR wall phenomenon can be avoided, providing useful energy detection performance at very low SNR.

Initial experimental measurements were also presented that explore energy detection performance in a true receiver using practical hardware. Detection performance based on empirically measured pdfs indicated that useful detection down to at least -16 dB is possible with energy detection using sufficient integration time. Measured noise distributions over short (0.3 s) and moderate (58 s) acquisition times showed negligible deviation from a Chi-Squared distribution, suggesting that the noise level in our system is very stable and that detailed modeling of the noise uncertainty is unnecessary for sub-minute integration times.

Since only an expensive instrument-grade LNA was considered in this work, future work will explore noise variation in low-cost commercial-grade amplifiers that may exhibit noise statistics that are much less stable. Additionally, due to existing limitations of the system acquisition firmware, we could not explore the performance of very long acquisition times, which will also be the subject of future investigations.

References

[1] Mitola, J., III and Maguire, G. Q., Jr., "Cognitive radio: Making software radios more personal," *IEEE Personal Commun. Magazine*, vol. 6, pp. 13–18, Aug. 1999.

[2] R. Tandra and A. Sahai, "SNR walls for signal detection," *IEEE J. Selected Topics Signal Processing*, vol. 2, pp. 4–17, Feb. 2008.

[3] S. M. Kay, *Fundamentals of Statistical Signal Processing: Detection Theory*, vol. II, Prentice-Hall, 1998.

[4] B. T. Maharaj, J. W. Wallace, M. A. Jensen, and L. P. Linde, "A low-cost open-hardware wideband multiple-input multiple-output (MIMO) wireless channel sounder," *IEEE Trans. Instrum. Meas.*, vol. 57, pp. 2283 – 2289, Oct. 2008.